

# FTIN: Frequency-Time Integration Network for Inertial Odometry

Shanshan Zhang, Qi Zhang, Siyue Wang, Tianshui Wen, Ziheng Zhou, Lingxiang Zheng, Yu Yang

**Abstract**—In recent years, machine learning has achieved significant advancements in inertial odometry. However, most existing inertial odometry methods primarily rely on CNNs in the time domain. These methods often struggle to capture long-term dependency in inertial measurement unit data, thereby constraining the potential for further improvements in localization accuracy. To address these issues, we propose a novel network architecture that integrates both frequency-domain and time-domain information. Specifically, we leverage the global view and energy compaction properties of frequency-domain learning to effectively model long-term dependency and reduce redundancy in IMU data. Additionally, we introduce a Scalar LSTM to capture sequential dependencies in the time domain, enabling cross-domain information fusion and providing a stable and reliable reference for localization. Experimental evaluations on multiple public datasets (e.g., RIDI, RoNIN, OxIOD, RNIN, TLIO, and IMUNet) demonstrate the effectiveness of the proposed frequency-time domain fusion strategy. Notably, on the RoNIN dataset, our method achieves a 43.0% reduction in absolute trajectory error and a 13.1% reduction in relative trajectory error compared to RoNIN ResNet.

**Index Terms**—Inertial Odometry, Frequency-Domain Learning, Cross-domain Information Mixing

## I. INTRODUCTION

**T**HE Inertial Measurement Unit (IMU), consisting of a three-axis accelerometer and a three-axis gyroscope, provides stable and high-frequency measurements (typically exceeding 100 Hz) of the carrier’s acceleration and angular velocity. Compared to visual and radar systems, IMUs offer several key advantages, including independence from environmental conditions, low cost, and high sampling rates. These characteristics make IMUs widely applicable in scenarios such as autonomous driving, disaster response, and other location-based services [1]–[5].

Inertial Odometry (IO) aims to estimate the position of a carrier using IMU measurements. Existing methods are typically based on either Newtonian mechanics or machine learning techniques operating in the time domain. Newtonian mechanics-based methods do not require large amounts of labeled data or computational resources. However, they often impose constraints on usage scenarios or sensor placements, limiting their applicability in complex motion environments such as the outdoors [6]. For instance, the Pedestrian Dead Reckoning (PDR) [7] estimates position based on stride length and heading direction, but it requires users to maintain a consistent gait.

In recent years, machine learning-based methods have significantly advanced IO, improving its positioning accuracy and broadening its applicability [8], [9]. A common strategy involves leveraging the local feature extraction capabilities of convolutional neural networks (CNNs) to model motion variations in IMU data. For instance, RoNIN [6] directly estimates

velocity from time-domain IMU signals using ResNet [10], while IMUNet [11] enhances performance on mobile devices through a lightweight network design.

However, CNN-based IO approaches often struggle to capture the contextual motion information embedded in IMU sequences, which limits their positioning accuracy. To address this, researchers have combined CNNs with LSTM networks or attention mechanisms [12] to model global motion trends, as demonstrated by methods such as RNIN [13], SSHNN [14], and SCHNN [15]. Nonetheless, these approaches tend to overlook the information bottleneck problem in high-frequency IMU signals, which hampers the accurate reconstruction of motion trajectories.

From a frequency-domain perspective, attention mechanisms—operating globally by design—are particularly effective at extracting low-frequency components that convey global contextual information [16], [17].

Beyond the scope of IO, both theoretical analyses and empirical studies on time-series modeling have shown that frequency-domain learning provides global representations that facilitate the modeling of long-term dependencies [18]. Moreover, this perspective emphasizes a small number of dominant frequency components, reducing redundancy and improving representational efficiency.

Motivated by these insights, we propose transforming IMU signals into the frequency domain to enhance the modeling of long-term temporal dependencies. This transformation leverages the global temporal context inherent in the frequency domain and exploits the concentration of signal energy in dominant frequencies. As a result, critical motion patterns become more salient, enabling more effective feature extraction.

The main contributions of this work are summarized as follows:

- We reinterpret IMU data from a frequency-domain perspective, leveraging its global temporal context and the concentration of signal energy in a limited number of frequency components. This reduces redundancy and facilitates the modeling of long-term dependencies in IMU sequences;
- We extend the ResNet architecture with frequency-domain learning to integrate local motion features with global temporal dependencies;
- We introduce a Scalar LSTM module that enhances the model’s ability to capture long-term dependencies in the time domain, enabling effective cross-domain information fusion;
- We conduct extensive experiments on multiple public datasets and demonstrate that the proposed method significantly improves the accuracy of inertial odometry.

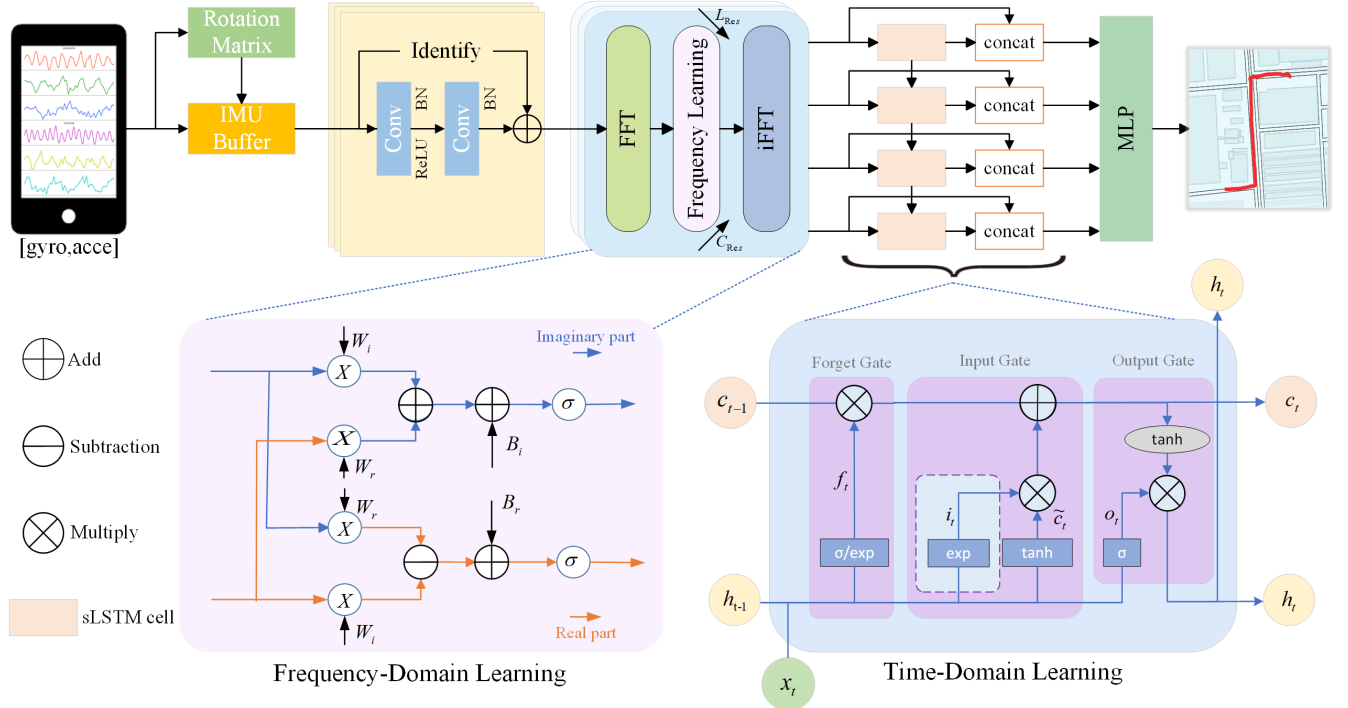


Fig. 1. The overall architecture of the proposed FTIN includes three stages: ResNet-1d, Frequency-Domain Learning (FDL), and Time-Domain Learning (TDL), which realizes cross-domain information fusion.

## II. RELATED WORK

To the best of our knowledge, current inertial odometry methods primarily rely on either Newtonian mechanics or machine learning techniques in the time domain.

The Strapdown Inertial Navigation System (SINS) [19] estimates position via double integration and depends on high-precision IMUs, which are typically expensive. Although approaches such as [20] have improved accuracy, error accumulation from double integration continues to undermine localization reliability during long-duration motion.

In smartphones, Step Counting (SC) is commonly used to estimate displacement, calculated as the product of a pre-defined step length and the number of detected steps [21]. Pedestrian Dead Reckoning (PDR) introduces algorithms for gait detection and step length estimation, assuming the user maintains a regular walking pattern [7]. Zero-Velocity Update (ZUPT) constrains the IMU to the foot and utilizes the zero-velocity condition during stance phases to correct drift [22]. Building on this, [23] proposes a Coriolis-based Heading Estimation (CHE) method to reduce heading errors in ZUPT-aided foot-mounted inertial navigation systems.

In recent years, machine learning approaches have gained prominence in IO research [4], [8], [24], [25]. RIDI [26] and PDRNet [27] first classify device placement and then apply specific models to regress position. IONet [28] and RoNIN [6] eliminate the need to distinguish between device placements or motion modes by directly estimating localization outputs from IMU data using unified network architectures. In particular, RoNIN incorporates ResNet, LSTM, and TCN models to regress 2D velocity, laying the foundation for subsequent works. Building upon RoNIN, TLIO [29] estimates

displacement and its uncertainty using ResNet, followed by stochastic cloning EKF (SCEKF) for filtering. Similarly, RNIN [13] extends ResNet with LSTM. LIDR [30] adopts a 1D variant of ResNet-18 as the encoder and tightly couples it with a Left-Invariant Extended Kalman Filter (LIEKF) to improve robustness under sudden lighting changes. SCHNN [15] and SSHNN [14] utilize CNN to capture local features and RNN to model long-term dependencies. Attention mechanisms are embedded in both CNN and RNN modules to enhance representational capacity. CTIN [31] and iMOT [32] introduce Transformer-based architectures specifically designed for inertial odometry, enabling accurate position estimation from IMU measurements. DIO [33] proposes random direction initialization during training to reduce reliance on device orientation. RIO [34] introduces rotational equivariance as a self-supervised strategy to enhance generalization and facilitate learning from unlabeled data. EqNIO [35] incorporates canonical displacement priors to address data variance caused by differing IMU orientations and motion directions, leveraging priors that are invariant in gravity-aligned frames. WDSNet [36] applies wavelet-based signal selection before ResNet inference to enhance signal quality and improve localization performance.

## III. METHOD

In this section, we introduce the overall architecture of the proposed FTIN model, followed by implementation details and a description of how long-term dependencies in both the frequency and time domains are captured.

TABLE I  
DESCRIPTION OF PUBLIC DATASETS USED FOR EVALUATION OF  
LOCALIZATION MODELS.

Dataset	IMU Carrier	Duration(hours)
RoNIN	Galaxy S9,Pixel 2 XL	42.7
RIDI	Lenovo Phab2 Pro	11.6
RNIN	Kaarta Stencil/smartphones	27.0
TLIO	Custom rig	60.0
OxIOD	iPhones,Nexus 5	14.7
IMUNet	Android phones	9.0

### A. Overall Structure

The overview of the proposed FTIN model pipeline is shown in Fig. 1. Given IMU data within a time window, denoted as  $X^{1:L} = [x_t^T, \dots, x_{t+L-1}^T] \in \mathbb{R}^{C \times L}$ , where  $x_t = [\text{acce}_t, \text{gyro}_t] \in \mathbb{R}^{1 \times C}$  represents the tri-axial acceleration and angular velocity at time  $t$ ,  $C$  denotes the number of feature channels (i.e., 3-axis acceleration and 3-axis angular velocity, hence  $C = 6$ ), and  $L$  is the window length.

The network backbone processes the IMU sequence through three successive stages to extract latent motion features. Lower layers primarily capture high-frequency local patterns, whereas higher layers focus on modeling low-frequency, long-term dependencies [17]. To this end, we first apply a ResNet-1d to extract fine-grained motion features and project them into a higher-dimensional space, thereby facilitating more effective modeling in subsequent stages. In the second stage, a Fourier transform is applied to convert the features into the frequency domain, followed by the use of Multilayer Perceptron (MLP) to learn long-term dependencies. This strategy leverages the global temporal context available in the frequency domain and capitalizes on the fact that signal energy is typically concentrated in a small number of frequency components. The strategy is performed independently along the channel and temporal dimensions, allowing the model to capture multidimensional long-term dependencies. Given that temporal modeling remains crucial for sequence-based tasks, we introduce a Scalar LSTM (sLSTM) [37] module in the third stage to capture long-term dependency in the time domain. Its scalar update mechanism preserves essential temporal information over extended sequences, thereby enhancing the model's ability to learn sequential patterns.

Finally, a three-layer MLP is employed to map the learned representations to 2D velocity estimates. The model is trained by minimizing the mean squared error (MSE) loss:

$$\text{MSE} = \frac{1}{N} \sum_{i=1}^N (v_i - \hat{v}_i)^2 \quad (1)$$

where  $N$  denotes the number of samples,  $v_i$  is the ground-truth velocity of the  $i$ -th sample, and  $\hat{v}_i$  is the corresponding predicted velocity.

### B. Frequency-Domain Learning

Attention mechanisms offer an effective means of capturing long-term dependencies in IMU data. From a frequency-domain perspective, attention mechanisms primarily target the

low-frequency components of the input signal [17]. Prior research has demonstrated that frequency-domain learning provides advantages such as a global view and energy compaction [18]. Motivated by these insights, we propose transforming the IMU data into the frequency-domain to more efficiently model long-term dependencies.

Specifically, since deeper layers in neural networks are more capable of modeling low-frequency components [17], we first apply a 1D ResNet to extract local, high-frequency, fine-grained motion features and project them into a higher-dimensional space.

Given the output  $X_{\text{Res}} \in \mathbb{R}^{C_{\text{Res}} \times L_{\text{Res}}}$  from the 1D ResNet, we introduce an additional embedding dimension  $d$  to facilitate frequency-domain learning:

$$X_{\text{tokenEmb}} = \text{reshape}(X_{\text{Res}}) \times W_1 \in \mathbb{R}^{C_{\text{Res}} \times L_{\text{Res}} \times d} \quad (2)$$

where  $\text{reshape}(\cdot)$  inserts the new embedding dimension without altering the original data values, and  $W_1 \in \mathbb{R}^{1 \times d}$  is a learnable weight matrix.

For the input  $x_{\text{tokenEmb}}^l \in \mathbb{R}^{C_{\text{Res}} \times d}$  at the  $l$ -th time step, we apply the Fourier transform along the channel dimension:

$$x(f)^l_{\text{channel}} = \frac{1}{\sqrt{N_c}} \sum_{c=0}^{N_c-1} x_{\text{tokenEmb}}^l(c) e^{-j \frac{2\pi}{N_c} cf} \quad (3)$$

where  $f$  is the frequency index,  $c$  the channel index, and  $N_c$  the total number of channels. Due to the conjugate symmetry of real-valued signals, only the first half of the spectrum is retained. The resulting representation  $x(f)^l_{\text{channel}} \in \mathbb{R}^{(C_{\text{Res}}/2) \times d}$  captures frequency-domain features.

To model inter-channel dependencies, we apply MLPs that separately transforms the real and imaginary components:

$$\begin{aligned} y^0 &= x(f)^n_{\text{channel}}, n = 0 \\ y^n &= \sigma(\mathbf{R}(y^{n-1})W_r^n - \mathbf{I}(y^{n-1})W_i^n + B_r^n) \\ &\quad + j\sigma(\mathbf{R}(y^{n-1})W_i^n + \mathbf{I}(y^{n-1})W_r^n + B_i^n), n > 0 \end{aligned} \quad (4)$$

where  $W^n = W_r^n + jW_i^n \in \mathbb{R}^{d \times d}$  and  $B^n = B_r^n + jB_i^n \in \mathbb{R}^d$  are complex-valued weight matrices and biases for the  $n$ -th layer, and  $\sigma(\cdot)$  denotes the activation function.

An inverse Fourier transform is then applied to reconstruct the time-domain representation:

$$z^n(c) = \frac{1}{\sqrt{N_c}} \sum_{f=0}^{N_c-1} y^n(f) e^{j \frac{2\pi}{N_c} cf} \quad (5)$$

where  $z^n(c) \in \mathbb{R}^{C_{\text{Res}} \times d}$  denotes the recovered features in the time domain. Aggregating over all time steps yields  $Z(c) \in \mathbb{R}^{C_{\text{Res}} \times L_{\text{Res}} \times d}$ .

Similarly, to capture inter-temporal dependencies, we perform a frequency transformation along the temporal dimension on the input  $z^c \in \mathbb{R}^{L_{\text{Res}} \times d}$  for each channel  $c$ . The resulting features are denoted as  $X_{\text{fre}} \in \mathbb{R}^{C_{\text{Res}} \times L_{\text{Res}} \times d}$ .

Finally, we flatten the temporal and embedding dimensions to obtain  $X_{\text{fre}} \in \mathbb{R}^{C_{\text{fre}} \times (L_{\text{Res}} \times d)}$ , followed by a fully connected layer and a non-linear activation to enhance representational capacity. The final output of the frequency-domain module is denoted as  $X_{\text{fre}} \in \mathbb{R}^{C_{\text{fre}} \times L_{\text{fre}}}$ , where  $C_{\text{fre}}$  and  $L_{\text{fre}}$  are the output channel and temporal dimensions, respectively.

TABLE II  
OVERALL TRAJECTORY PREDICTION ACCURACY (UNITS OF ALL METRICS ARE IN METER). THE BEST RESULT IS PRESENTED IN BOLD FONT.

Datasets	Metric	Method							FTIN improvement over RoNIN ResNet
		RoNIN ResNet	RoNIN LSTM	RoNIN TCN	RNIN	IMUNet	sTLIO	Ours	
RoNIN	ATE	6.799	6.136	5.500	5.686	5.550	4.417	<b>3.875</b>	43.0%
	RTE	3.523	3.595	3.563	3.449	3.387	3.507	<b>3.061</b>	13.1%
RIDI	ATE	2.608	3.294	2.743	1.851	2.645	2.641	<b>1.727</b>	33.8%
	RTE	2.881	3.136	2.476	2.040	2.788	3.105	<b>1.981</b>	31.2%
RNIN	ATE	1.182	1.893	1.561	1.143	1.417	1.493	<b>1.096</b>	7.3%
	RTE	2.036	2.732	2.108	1.251	1.872	1.493	<b>1.114</b>	45.3%
TLIO	ATE	1.445	2.087	4.682	1.611	<b>1.432</b>	1.779	1.479	-2.4%
	RTE	3.758	5.990	14.524	4.637	<b>3.474</b>	5.127	3.552	5.5%
OxIOD	ATE	3.557	4.277	26.442	4.343	9.822	5.071	<b>3.446</b>	3.1%
	RTE	1.324	1.683	5.628	1.340	2.307	1.445	<b>1.165</b>	12.0%
IMUNet	ATE	18.040	10.182	38.272	16.552	11.847	17.190	<b>10.171</b>	43.6%
	RTE	9.251	7.382	29.620	8.566	7.792	9.312	<b>7.289</b>	21.2%

Through the coordinated operation of these components, the model emphasizes the most informative frequency components, reduces redundancy, and effectively captures long-term dependencies across both the channel and temporal dimensions. This establishes a strong foundation for downstream localization tasks.

### C. Time-Domain Learning

While frequency-domain learning offers notable advantages, it does not eliminate the necessity of time-domain modeling. In fact, the combination of frequency- and time-domain processing is a well-established strategy for capturing long-term dependencies in sequential data. Since conventional LSTM architectures often suffer from issues such as vanishing gradients when modeling extended temporal dependencies, we introduce a Scalar LSTM (sLSTM) module following the frequency-domain learning stage. This module captures temporal dependencies in the IMU sequences, thereby enabling the integration of complementary information from both domains.

The sLSTM enhances long-term dependency modeling by optimizing its internal memory cell and employing a scalar update mechanism. This design improves the efficiency of sequential learning, facilitates cross-domain information fusion, and provides a stable and reliable reference for downstream localization tasks.

The output of the time-domain learning stage is defined as:

$$X_{\text{temp}} = \text{sLSTM}(X_{\text{fre}}) \in \mathbb{R}^{C_{\text{temp}} \times L_{\text{temp}}} \quad (6)$$

where  $\text{sLSTM}(\cdot)$  denotes the sequence modeling operation performed by the sLSTM module.

## IV. EXPERIMENTS AND ANALYSIS

### A. Experimental Settings

**Datasets.** Table I summarizes the basic characteristics of the publicly available datasets used in our experiments, including RIDI [26], RoNIN [6], OxIOD [38], RNIN [13], TLIO [29], and IMUNet [11]. These datasets encompass a wide range of collection scenarios, providing a comprehensive basis for

research and validation in inertial odometry. Prior to training, each dataset is randomly shuffled and split into training, validation, and testing sets in an 8:1:1 ratio to ensure fair and consistent evaluation.

**Baselines.** Compared to traditional Newtonian-based methods, machine learning approaches have demonstrated significant performance advantages. Therefore, we primarily compare several representative learning-based models, including the ResNet, LSTM, and TCN architectures introduced in RoNIN [6]; the lightweight IMUNet constructed with depthwise separable convolutions [11]; the full TLIO model and a variant of TLIO without the SCEKF (TLIO (w/o SCEKF)) [29]; and the RNIN models [13].

**Evaluation Metrics.** We adopt three widely used evaluation metrics to assess localization performance: Absolute Trajectory Error (ATE), Relative Trajectory Error (RTE), and Position Drift Error (PDE). ATE and RTE evaluate the model’s accuracy in predicting global and local trajectories, respectively [39]. Lower values of these metrics indicate better localization performance. PDE quantifies the drift error at the endpoint of the reconstructed trajectory [31].

**Training Details.** All experiments were conducted on a GPU-equipped system featuring an NVIDIA RTX A40 (48GB), with the runtime environment built using the official PyTorch Docker image. We set the batch size to 512, the maximum number of training epochs to 100, and the initial learning rate to  $10^{-4}$ . The Adam optimizer was employed for model training, and early stopping was applied when the learning rate dropped below  $10^{-6}$  to mitigate the risk of overfitting.

### B. Comparisons with the baselines

**Overall Performance.** Table II reports the ATE and RTE results for various models on the test datasets.

On the IMUNet dataset, FTIN performs comparably to RoNIN LSTM. On the RoNIN dataset, FTIN outperforms RoNIN ResNet, RoNIN LSTM, and RoNIN TCN, achieving reductions of 43.0% in ATE and 13.1% in RTE. Notably, the RoNIN architectures (ResNet, LSTM, and TCN), along with

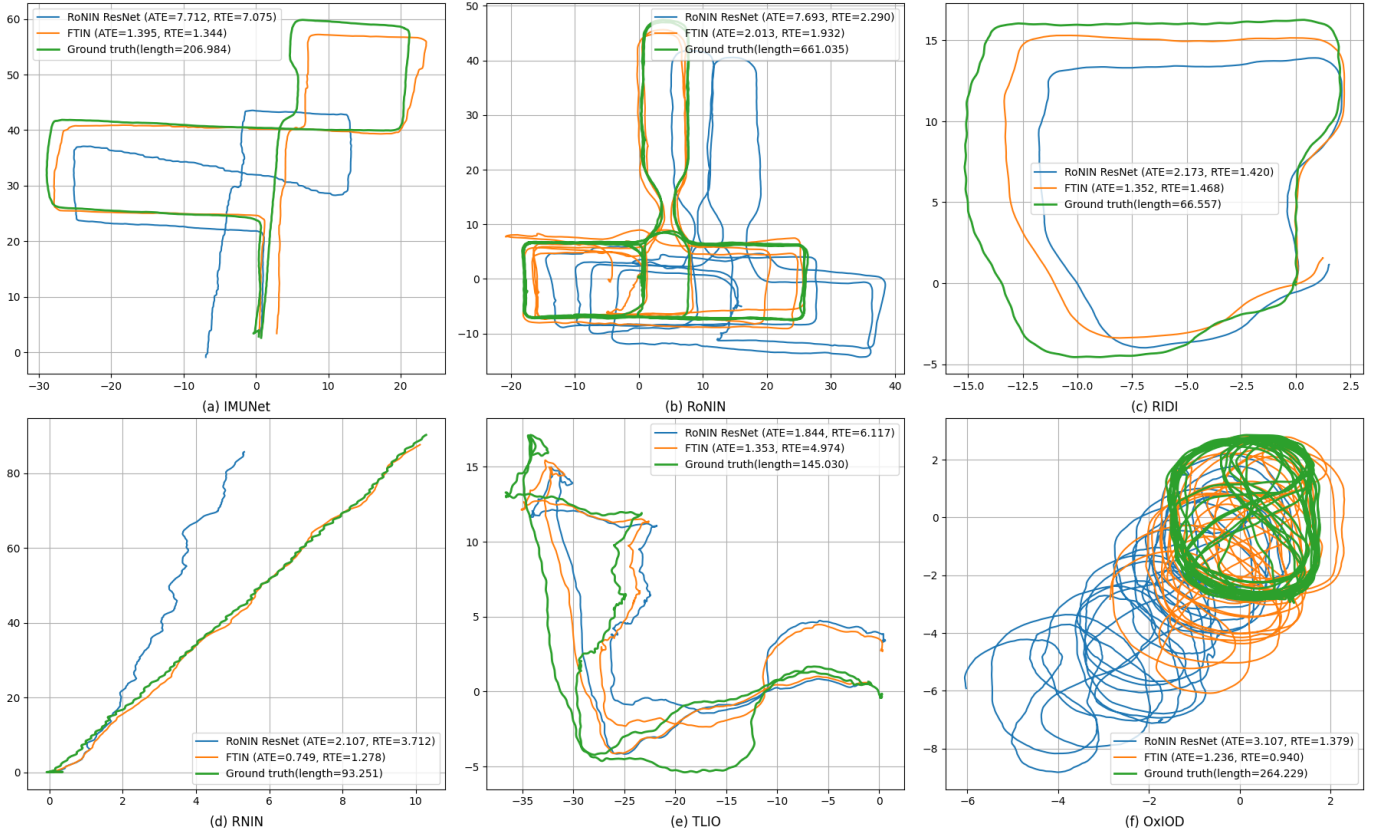


Fig. 2. Visual comparison of the proposed method and RoNIN ResNet on various datasets. In the figure, the axis titles, ATE, RTE, and trajectory length are all in meters. The dataset to which the trajectory belongs is indicated below each sub - figure.

RNIN, IMUNet, and TLIO, do not incorporate frequency-domain information, which limits their potential for further performance gains. RNIN, which combines ResNet and LSTM to enhance temporal modeling, achieves second-best results on the RIDI and RNIN datasets and performs competitively on the remaining datasets.

Overall, FTIN achieves substantial accuracy improvements across multiple benchmark datasets by jointly modeling time-domain and frequency-domain features, demonstrating its effectiveness for inertial odometry tasks.

**Visualization.** Fig. 2 presents a visual comparison between FTIN and the baseline models using representative trajectory samples from the test sets of each dataset. These samples include a range of scenarios, such as short-range movements and complex long-distance trajectories. A noticeable relationship between positioning accuracy and trajectory length is observed, with heading errors also significantly affecting localization performance.

In Fig. 2 (c) and (d), the accumulation of heading errors is clearly visible. However, for short-range movements, FTIN shows superior trajectory-fitting capability. In Fig. 2 (b) and (f), substantial rotational motion leads the baseline models to gradually deviate from the ground-truth trajectory. While FTIN demonstrates strong tracking performance in Fig. 2 (b), its performance in Fig. 2 (f) still leaves room for improvement. In other scenarios, FTIN generally provides accurate displacement estimation. These visual results further validate the effective-

ness of the combined time-domain and frequency-domain learning strategy in improving inertial odometry accuracy.

**Overall Model Behavior.** Fig. 3 presents the experimental results of FTIN in comparison with three baseline networks. Due to space constraints, only the results on the RoNIN dataset are reported. Fig. 3(a) and (b) respectively show the cumulative distribution function (CDF) curves for ATE and RTE of the selected networks. The FTIN curve (red) is noticeably steeper, indicating that FTIN achieves higher localization accuracy at the same ATE or RTE threshold than the other three networks. In addition, Fig. 3(c) illustrates the PDE for FTIN and the baseline methods. FTIN exhibits the lowest PDE value, suggesting that it can more accurately approximate the trajectory endpoint.

### C. Ablation Study

We further evaluate the performance of the proposed method on the open-source datasets used in the experiments, with a focus on analyzing the effectiveness of Frequency-Domain Learning (FDL) and Time-Domain Learning (TDL).

**Module Effectiveness.** FTIN uses a 1D ResNet as the backbone network for fine-grained motion feature extraction and dimensional mapping. The model then captures long-term dependencies in the IMU data in both the frequency and time domains, enabling cross-domain information fusion and improving the modeling capability of motion trajectories. Table III presents the ablation study results for different

TABLE III

OVERVIEW OF THE ABLATION STUDY. WE GRADUALLY EXCLUDE TIME-DOMAIN LEARNING (TDL) AND FREQUENCY-DOMAIN LEARNING (FDL) FROM FTIN TO VERIFY THE EFFECTIVENESS OF THE STRATEGY. THE BEST RESULT IS SHOWN IN BOLD FONT.  $\checkmark$  REPRESENTS INCLUSION, AND  $-$  REPRESENTS EXCLUSION. ALL THE METRICS ARE IN THE UNIT OF METERS.

Models	FDL	TDL	RoNIN		RIDI		RNIN		TLIO		OxIOD		IMUNet	
			ATE	RTE	ATE	RTE								
i	-	-	6.799	3.523	2.608	2.881	1.182	2.036	1.445	3.758	3.557	1.324	18.040	9.251
ii	$\checkmark$	-	5.877	3.323	1.962	2.194	1.193	1.199	<b>1.383</b>	3.595	3.518	1.308	14.610	8.598
iii	-	$\checkmark$	4.690	3.223	2.367	2.560	1.097	1.123	1.448	3.707	3.452	1.165	17.557	7.809
iv	$\checkmark$	$\checkmark$	<b>3.875</b>	<b>3.061</b>	<b>1.727</b>	<b>1.981</b>	<b>1.096</b>	<b>1.114</b>	1.479	<b>3.552</b>	<b>3.446</b>	<b>1.165</b>	<b>10.171</b>	<b>7.289</b>

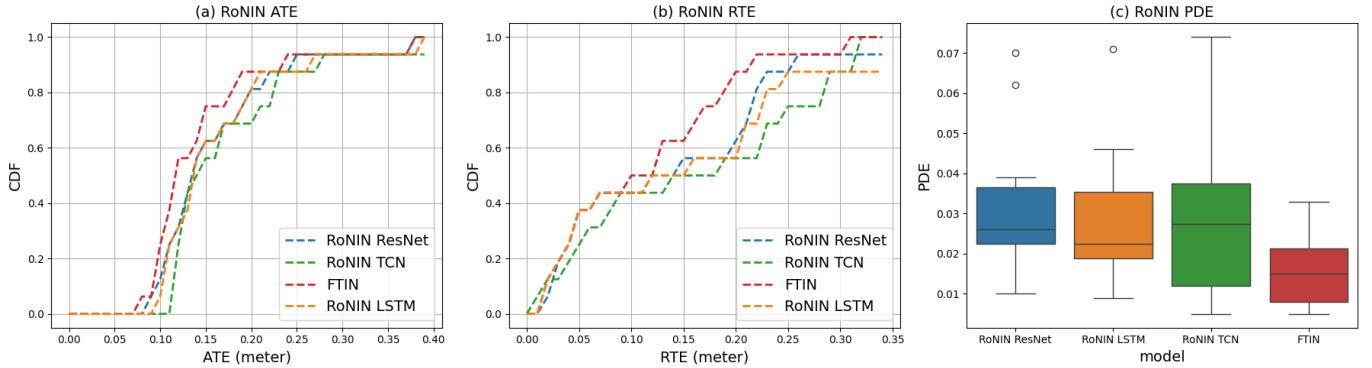


Fig. 3. (a) and (b) illustrate the Cumulative Density Functions (CDFs) of the proposed method (FTIN) compared with three baseline models from RoNIN on the RoNIN dataset. (c) reports the Position Drift Error (PDE) metric for the same set of methods.

modules on the open-source datasets used in the experiments. We progressively remove the FDL and TDL modules from FTIN, and the results show that both FDL and TDL independently enhance the model’s trajectory reconstruction ability, reducing ATE and RTE. Moreover, when both FDL and TDL are integrated, all datasets, except for the TLIO dataset, exhibit lower localization errors, validating the effectiveness and complementarity of FDL and TDL. The results on the TLIO dataset are still constrained by the gravity component in the dataset.

## V. CONCLUSION

We proposed a fusion of frequency-domain and time-domain information, with a focus on the frequency domain, to better capture the rich information embedded in inertial measurement data and achieve more accurate motion trajectory reconstruction. A key limitation of FTIN is the accumulation of heading errors, particularly when dealing with repetitive rotational movements, which leaves room for further improvement. Future work will explore the integration of a heading estimation mechanism to enhance the robustness of FTIN. Additionally, incorporating uncertainty information during model inference to improve localization accuracy will be an important avenue for future research.

## REFERENCES

- [1] N. Cohen and I. Klein, “Inertial navigation meets deep learning: A survey of current trends and future directions,” *Results in Engineering*, vol. 24, p. 103565, 2024. [Online]. Available: <https://www.sciencedirect.com/science/article/pii/S2590123024018085>
- [2] M. Freydin and B. Or, “Learning car speed using inertial sensors for dead reckoning navigation,” *IEEE Sensors Letters*, vol. 6, no. 9, pp. 1–4, 2022.
- [3] R. Fu, Q. Niu, M. Kou, Q. He, and N. Liu, “Aio: Enhancing generalization of inertial odometry to unseen scenarios with active learning,” in *2024 International Symposium on Digital Home (ISDH)*, 2024, pp. 155–160.
- [4] S. S. Saha, S. S. Sandha, L. A. Garcia, and M. Srivastava, “Tinyodom: Hardware-aware efficient neural inertial navigation,” *Proc. ACM Interact. Mob. Wearable Ubiquitous Technol.*, vol. 6, no. 2, Jul. 2022. [Online]. Available: <https://doi.org/10.1145/3534594>
- [5] C. Chen and X. Pan, “Deep learning for inertial positioning: A survey,” *IEEE Transactions on Intelligent Transportation Systems*, vol. 25, no. 9, pp. 10 506–10 523, 2024.
- [6] S. Herath, H. Yan, and Y. Furukawa, “Ronin: Robust neural inertial navigation in the wild: Benchmark, evaluations, & new methods,” in *2020 IEEE International Conference on Robotics and Automation (ICRA)*, 2020, pp. 3146–3152.
- [7] A. Nayak, A. Eskandarian, Z. Doerzaph, and P. Ghorai, “Pedestrian trajectory forecasting using deep ensembles under sensing uncertainty,” *IEEE Transactions on Intelligent Transportation Systems*, vol. 25, no. 9, pp. 11 317–11 329, 2024.
- [8] A. K. Panja, C. Chowdhury, and S. Neogy, “Survey on inertial sensor-based ils for smartphone users,” *CCF Transactions on Pervasive Computing and Interaction*, vol. 4, no. 3, pp. 319–337, 2022.
- [9] Y. Qiu, C. Xu, Y. Chen, S. Zhao, J. Geng, and S. Scherer, “Airio: Learning inertial odometry with enhanced imu feature observability,” *IEEE Robotics and Automation Letters*, pp. 1–8, 2025.
- [10] K. He, X. Zhang, S. Ren, and J. Sun, “Deep residual learning for image recognition,” in *Proceedings of the 2016 IEEE Conference on Computer Vision and Pattern Recognition (CVPR)*, 2016, pp. 770–778.
- [11] B. Zeinali, H. Zanddizari, and M. J. Chang, “Imunet: Efficient regression architecture for inertial imu navigation and positioning,” *IEEE Transactions on Instrumentation and Measurement*, vol. 73, no. 2516213, 2024.
- [12] A. Vaswani, N. Shazeer, N. Parmar, J. Uszkoreit, L. Jones, A. N. Gomez, L. Kaiser, and I. Polosukhin, “Attention is all you need,” in *Proceedings of the 31st International Conference on Neural Information Processing Systems*, ser. NIPS’17. Red Hook, NY, USA: Curran Associates Inc., 2017, p. 6000–6010.
- [13] D. Chen, N. Wang, R. Xu, W. Xie, H. Bao, and G. Zhang, “Rninvio: Robust neural inertial navigation aided visual-inertial odometry in

- challenging scenes,” in *2021 IEEE International Symposium on Mixed and Augmented Reality (ISMAR)*, 2021, pp. 275–283.
- [14] Y. Wang, H. Cheng, A. Zhang, and M. Q.-H. Meng, “From imu measurement sequence to velocity estimate sequence: An effective and efficient data-driven inertial odometry approach,” *IEEE Sensors Journal*, vol. 23, no. 15, pp. 17 117–17 126, 2023.
- [15] Y. Wang, H. Cheng, and M. Q.-H. Meng, “Spatiotemporal co-attention hybrid neural network for pedestrian localization based on 6d imu,” *IEEE Transactions on Automation Science and Engineering*, vol. 20, no. 1, pp. 636–648, 2023.
- [16] F. Chollet, “Xception: Deep learning with depthwise separable convolutions,” in *2017 IEEE Conference on Computer Vision and Pattern Recognition (CVPR)*, 2017, pp. 1800–1807.
- [17] C. Si, W. Yu, P. Zhou, Y. Zhou, X. Wang, and S. Yan, “Inception transformer,” in *Proceedings of the 36th International Conference on Neural Information Processing Systems*, ser. NIPS ’22. Red Hook, NY, USA: Curran Associates Inc., 2022.
- [18] K. Yi, Q. Zhang, W. Fan, S. Wang, P. Wang, H. He, N. An, D. Lian, L. Cao, and Z. Niu, “Frequency-domain MLPs are more effective learners in time series forecasting,” in *Thirty-seventh Conference on Neural Information Processing Systems*, 2023.
- [19] P. G. Savage, “Strapdown inertial navigation integration algorithm design part 2: Velocity and position algorithms,” *Journal of Guidance, Control, and Dynamics*, vol. 21, no. 2, pp. 208–221, 1998.
- [20] M. Yanling, X. Zhi, X. Li, L. Jianye, and Y. Dequan, “An improved method of sins/cns integrated navigation algorithm based on dual quaternions with gyro error corrected online,” in *2017 29th Chinese Control And Decision Conference (CCDC)*, 2017, pp. 179–184.
- [21] A. Brajdic and R. Harle, “Walk detection and step counting on unconstrained smartphones,” in *Proceedings of the 2013 ACM International Joint Conference on Pervasive and Ubiquitous Computing*, ser. UbiComp ’13. New York, NY, USA: Association for Computing Machinery, 2013, p. 225–234. [Online]. Available: <https://doi.org/10.1145/2493432.2493449>
- [22] R. P. Suresh, V. Sridhar, J. Pramod, and V. Talasila, “Zero velocity potential update (zupt) as a correction technique,” in *Proceedings of the 2018 3rd International Conference On Internet of Things: Smart Innovation and Usages (IoT-SIU)*, 2018, pp. 1–8.
- [23] Z. Li, Z. Deng, Z. Meng, and P. Zhang, “Coriolis-based heading estimation for pedestrian inertial localization based on mems mimu,” *IEEE Internet of Things Journal*, vol. 11, no. 16, pp. 27 509–27 517, 2024.
- [24] S. Herath, D. Caruso, C. Liu, Y. Chen, and Y. Furukawa, “Neural inertial localization,” in *2022 IEEE/CVF Conference on Computer Vision and Pattern Recognition (CVPR)*, 2022, pp. 6594–6603.
- [25] J. Liu, Z. Yang, S. Zlatanova, S. Li, and B. Yu, “Indoor localization methods for smartphones with multi-source sensors fusion: Tasks, challenges, strategies, and perspectives,” *Sensors*, vol. 25, no. 6, 2025. [Online]. Available: <https://www.mdpi.com/1424-8220/25/6/1806>
- [26] H. Yan, Q. Shan, and Y. Furukawa, “Ridi: Robust imu double integration,” in *Computer Vision – ECCV 2018*, V. Ferrari, M. Hebert, C. Sminchisescu, and Y. Weiss, Eds. Cham: Springer International Publishing, 2018, pp. 641–656.
- [27] O. Asraf, F. Shama, and I. Klein, “Pdrnet: A deep-learning pedestrian dead reckoning framework,” *IEEE Sensors Journal*, vol. 22, no. 6, pp. 4932–4939, 2022.
- [28] C. Chen, X. Lu, A. Markham, and N. Trigoni, “Ionet: Learning to cure the curse of drift in inertial odometry,” in *Proceedings of the AAAI Conference on Artificial Intelligence*, vol. 32, no. 1, 2018.
- [29] W. Liu, D. Caruso, E. Ilg, J. Dong, A. I. Mourikis, K. Daniilidis, V. Kumar, and J. Engel, “Thio: Tight learned inertial odometry,” *IEEE Robotics and Automation Letters*, vol. 5, no. 4, pp. 5653–5660, 2020.
- [30] D. Yang, H. Liu, X. Jin, J. Chen, C. Wang, X. Ding, and K. Xu, “Enhancing vio robustness under sudden lighting variation: A learning-based imu dead-reckoning for uav localization,” *IEEE Robotics and Automation Letters*, vol. 9, no. 5, pp. 4535–4542, 2024.
- [31] B. Rao, E. Kazemi, Y. Ding, D. M. Shila, F. M. Tucker, and L. Wang, “Ctin: Robust contextual transformer network for inertial navigation,” *Proceedings of the AAAI Conference on Artificial Intelligence*, vol. 36, no. 5, pp. 5413–5421, Jun. 2022. [Online]. Available: <https://ojs.aaai.org/index.php/AAAI/article/view/20479>
- [32] S. M. Nguyen, L. D. Tran, D. Viet Le, and P. J. M. Havinga, “iMoT: Inertial Motion Transformer for Inertial Navigation,” *arXiv e-prints*, p. arXiv:2412.12190, Dec. 2024.
- [33] Y. Wang, H. Cheng, C. Wang, and M. Q.-H. Meng, “Pose-invariant inertial odometry for pedestrian localization,” *IEEE Transactions on Instrumentation and Measurement*, vol. 70, no. 8503512, 2021.
- [34] X. Cao, C. Zhou, D. Zeng, and Y. Wang, “Rio: Rotation-equivariance supervised learning of robust inertial odometry,” in *2022 IEEE/CVF Conference on Computer Vision and Pattern Recognition (CVPR)*, 2022, pp. 6604–6613.
- [35] R. K. Jayanth, Y. Xu, Z. Wang, E. Chatzikipantazis, K. Daniilidis, and D. Gehrig, “EqNIO: Subequivariant neural inertial odometry,” in *The Thirteenth International Conference on Learning Representations*, 2025. [Online]. Available: <https://openreview.net/forum?id=C8jXEugWkq>
- [36] Y. Wang and Y. Zhao, “Wavelet dynamic selection network for inertial sensor signal enhancement,” *Proceedings of the AAAI Conference on Artificial Intelligence*, vol. 38, no. 14, pp. 15 680–15 688, Mar. 2024. [Online]. Available: <https://ojs.aaai.org/index.php/AAAI/article/view/29496>
- [37] M. Beck, K. Pöppel, M. Spanring, A. Auer, O. Prudnikova, M. Kopp, G. Klambauer, J. Brandstetter, and S. Hochreiter, “xlstm: Extended long short-term memory,” in *Thirty-eighth Conference on Neural Information Processing Systems*, 2024. [Online]. Available: <https://arxiv.org/abs/2405.04517>
- [38] C. Chen, P. Zhao, C. X. Lu, W. Wang, A. Markham, and N. Trigoni, “Oxiod: The dataset for deep inertial odometry,” *arXiv preprint arXiv:1809.07491*, 2018.
- [39] J. Sturm, N. Engelhard, F. Endres, W. Burgard, and D. Cremers, “A benchmark for the evaluation of rgb-d slam systems,” in *Proceedings of the 2012 IEEE/RSJ International Conference on Intelligent Robots and Systems*, 2012, pp. 573–580.